Chinese Journal of Physiology 61(1): 1-13, 2018
DOI: 10.4077/CJP.2018.BAG516

Stimulatory Action of Telmisartan, an Antagonist of Angiotensin II Receptor, on Voltage-Gated Na^+ Current: Experimental and Theoretical Studies

Tzu-Tung Chang, Chia-Jung Yang, Yu-Chi Lee, and Sheng-Nan Wu

Department of Physiology, National Cheng Kung University Medical College, Tainan 70101, Taiwan, Republic of China

Abstract

Telmisartan (Tel) is recognized as a non-peptide blocker of AT1R. Whether this agent has any direct effects on ion currents remains unexplored. In whole-cell current recordings, addition of Tel increased the peak amplitude of voltage-gated Na^+ (Na_V) current (I_{Na}) accompanied by the increased time constant of I_{Na} inactivation in differentiated NSC-34 motor neuron-like cells. Tel-stimulated I_{Na} in these cells is unlinked to either blockade of AT1R or activation of peroxisome proliferator-activated receptor gamma (PPAR-γ). In order to explore how this compound affects the amplitude and kinetics of I_{Na} in neurons, a Hodgkin-Huxley-based (HH-based) model designed to mimic effect of Tel on the functional activities of neurons was computationally created in this study. In this framework, the parameter for *h* inactivation gating variable, which was changed in a stepwise fashion, was implemented to predict changes in membrane potentials (*V*) as a function of maximal Na^+ (G_{Na}), K^+ conductance (G_K), or both. As inactivation time course of I_{Na} was increased, the bifurcation point of *V* versus G_{Na} became lower, and the range between subcritical and supercritical values at the bifurcation of *V* versus G_K correspondingly became larger. During a slowing in I_{Na} inactivation, the critical boundary between G_{Na} and G_K was shifted towards the left. Simulation studies demonstrated that progressive slowing in the inactivation time course of I_{Na} resulted in unanticipated increase of neuronal excitability by mimicking the effect of Tel in neuronal cells. Collectively, Tel can directly interact with the Na_V channel to increase peak I_{Na} as well as to slow I_{Na} inactivation. It is thus highly likely that the effects of Tel or its structurally similar drugs could be another intriguing mechanism underlying their pharmacological actions in neurons or neuroendocrine cells occurring *in vivo*.

Key Words: bifurcation analysis, Hodgkin-Huxley kinetics, potassium current, sodium current, Telmisartan

Introduction

Telmisartan (Tel), a non-peptide, orally-active blocker of AT1R, is the newest available drug class which has been widely used for treating hypertension and different cardiovascular disorders (2, 10, 43). Because Tel has a distinctive aromatic group that is modified, it possesses good lipophilicity so as to readily transverse the blood-brain barrier and subsequently to penetrate different brain regions (26). Moreover, owing to its activation of peroxisome proliferator-activated receptor gamma (PPAR-γ) ac-

Corresponding author: Dr. Sheng-Nan Wu, Department of Physiology, National Cheng Kung University Medical College, No. 1, University Road, Tainan 70101, Taiwan, ROC. Tel: +886-6-2353535-5334; Fax: +886-6-2362780; E-mail: snwu@mail.ncku.edu.tw
Received: March 6, 2017; Revised (Final Version): July 6, 2017; Accepted: July 12, 2017.
 ISSN : 0304-4920. http://www.cps.org.tw

tivity or blockade of angiotensin II receptor (3, 29), there is a considerable body of evidence to show the ability of this compound to produce anti-inflammatory actions (1, 2, 19), to ameliorate impaired cognitive functions (8, 13, 23) and to be beneficial for traumatic or ischemic brain injuries (19, 20, 22, 29-31).

The voltage-gated Na^+ (Na_V) channels, nine subtypes of which were denoted $Na_V1.1$ through $Na_V1.9$, belong to the larger protein superfamily of voltage-dependent ion channels and they are involved in the generations and propagation of action potentials (APs) in electrically excitable cells (5). Once the membrane is adequately depolarized, Na_V channels can readily go through rapid transitions from their resting to the open state, then to the inactivated state. The genetic defects in Na^+ channel inactivation that result in small sustained Na^+ current (I_{Na}) after the AP firing have been recognized to have devastating consequences, including seizures, periodic paralysis, neuropathic pain, and long QT-3 (LQT-3) syndrome (11, 17, 21, 25, 33). Of interest, an earlier work showed the ability of Tel to retard the inactivation of I_{Na} in rat cardiomyocytes (18). Previous observations at our laboratory have demonstrated the presence of I_{Na} in differentiated NSC-34 motor neuron-like cells (39). However, to what extent this compound has any direct perturbations on ion-channel activity in neurons or neuroendocrine cells remains incompletely understood.

For these reasons, the aim of this study was to use an experimental and simulation approach for evaluation of the role of Na_V-channel kinetics in the electrical behavior of neurons and for investigations of the observed effects of Tel on I_{Na} in NSC-34 neuronal cells. In this study, we found that, aside from its blockade of AT1Rs or stimulation of PPAR-γ activity, Tel is particularly effective not only at stimulating the peak amplitude of I_{Na} but also at delaying I_{Na} inactivation. Additionally, by capturing the qualitative aspects of the issue how the gating kinetics of I_{Na} influence electrical behaviors of neurons, numerical simulations of this current were noted to reproduce the actual experimental data and showed that changes in AP firing caused by this compound could arise from both increase in the peak amplitude and inactivation time constant of I_{Na}.

Materials and Methods

Cell Preparations

NSC-34 neuronal cells were originally produced by fusion of motor neuron-enriched, embryonic mouse spinal cords with mouse neuroblastoma. Briefly, they were maintained in 1:1 mixture of Dulbecco's modified Eagle's medium (DMEM) and Ham's F-12 medium supplemented with 10% (v/v) fetal bovine serum (FBS) and 1% penicillin-streptomycin (15, 39). Cultures were incubated at 37°C in a humidified environment of 5% CO_2/95% air. The medium was replenished every 2-3 days for removal of non-adhering cells. To slow cell proliferation and enhance their maturation towards a differentiated state, before confluence, cells were grown in 1:1 DMEM plus Ham's F-12 medium supplemented with 1% FBS. In a separate set of experiments, NSC-34 cells were treated with angiotensin II (200 nM) at 37°C for six hours.

Electrophysiological Measurements

Shortly before the experiments were made, NSC-34 cells were harvested with 1% trypsin/ethylenediaminetetraacetic acid (EDTA) solution and an aliquot of cell suspension was thereafter transferred to a home-made recording chamber mounted on the stage of a DM-IL inverted microscope (Leica Microsystems, Wetzlar, Germany). They were bathed at room temperature (20-25°C) in normal Tyrode's solution to which 1.8 mM $CaCl_2$ was added. The composition of Hepes-buffered normal Tyrode's solution was as follows (in mM): NaCl 136.5, KCl 5.4, $CaCl_2$ 1.8, $MgCl_2$ 0.53, glucose 5.5, and Hepes-NaOH buffer 5 (pH 7.4). To record K^+ current, recording pipette was filled with a solution (in mM): KCl 140, $MgCl_2$ 1, Na_2ATP 3, Na_2GTP 0.1, EGTA 0.1, and Hepes-KOH buffer 5 (pH 7.2). To measure I_{Na}, K^+ ions inside the internal solution were replaced with equimolar Cs^+ ions, and the pH was adjusted to 7.2 with CsOH. Patch pipettes were pulled from Kmax-51 glass capillaries (#34500; Kimble Glass, Vineland, NJ) using either a PP-830 puller (Narishige, Tokyo, Japan) or a P-97 Flaming/Brown micropipette puller (Sutter, Novato, CA), and they were then fire-polished with an MF-83 microforge (Narishige). The electrodes, which bore resistances between 3 and 5 MΩ when filled with different intracellular solutions, were maneuvered by use of an MX-4 manipulator (Narishige) precisely controlled by an MHW-3 hydraulic micromanipulator (Narishige). Standard patch-clamp recordings were performed in whole-cell configuration of the patch-clamp technique by means of an RK-400 (Bio-Logic, Claix, France) or Axopatch-200B (Molecular Devices, Sunnyvale, CA) patch-clamp amplifier (21, 39).

Data Recordings and Analyses

The signals were displayed on a liquid crystal projector (PJ550-2; ViewSonic, Walnut, CA, USA) and online stored in a TravelMate-6253 laptop computer (Acer, Taipei, Taiwan) at 10 kHz through a DigiData-1320 series interface (Molecular Devices).

The latter device was equipped with an Adaptec SlimSCSI card (Milpitas, CA, USA) *via* a PCMCIA card slot and mainly controlled by pCLAMP 9.2 (Molecular Devices). In some set of experiments, the data were acquired by PowerLab acquisition system with LabChart 7.0 software (AD Instruments; Gerin, Tainan, Taiwan). Ion currents were low-pass filtered at 1-3 kHz. The signals achieved during whole-cell experiments were offline analyzed using pCLAMP 9.2 (Molecular Devices), Origin 8.0 (OriginLab, Northampton, MA), or custom-made macros built in Excel 2013 spreadsheet running on Windows-8 (Microsoft, Redmond, WA, USA). To determine the current-voltage relationships and the steady-state activation or inactivation curves for ion currents (*e.g.*, I_{Na}), a family of rectangular or ramp voltage pulses generated by pCLAMP 9.2 were digitally created.

To evaluate the percentage stimulation of Tel on peak I_{Na}, cells were bathed in Ca^{2+}-free Tyrode's solution, each cell was depolarized from -80 to -10 mV, and peak amplitude during different concentrations of Tel was compared. The peak amplitude of I_{Na} in the presence of 30 μM Tel was taken as 100%. The Tel concentration required to stimulate 50% of current amplitude was fitted to a Hill function: $y = E_{max}/\{1+(EC_{50}^{n}/[C]^{n})\}$, where [C] is the concentration of Tel, EC_{50} and n are the half-maximal concentration of Tel required to stimulate I_{Na} and the Hill coefficient, respectively, and E_{max} is Tel-induced maximal stimulation of I_{Na}.

To characterize the steady-state inactivation curve of I_{Na} with or without addition of Tel, the two-step voltage profile was employed. The relationships between the conditioning potentials (from -100 to -10 mV with a duration of 50 msec) and the normalized amplitude of I_{Na} in response to membrane depolarization from -80 to -10 mV were plotted and well fit by the Boltzmann equation: $I/I_{max} = 1/\{1+\exp[(V-V_{1/2})/k]\}$, where I_{max} is the maximal activated I_{Na}, V the membrane potential in mV, $V_{1/2}$ the membrane potential for half-maximal inactivation, and k the slope factor of inactivation curve.

The trajectory of I_{Na} activation or inactivation elicited by step depolarization seen in NSC-34 neuronal cells was fitted by a one- or two-exponential process, respectively. The solver subroutine built in Microsoft Excel was used to fit the trajectory by least-squares minimization procedure. Results of experiments performed on NSC-34 cells shown in Fig. 1B, 1C and 1D are expressed as the mean ± standard error of the mean (SEM), and the values of *n* indicate the number of cells from which the data were taken. The paired or unpaired Student's *t* test and one-way analysis of variance with a least-significance difference method for multiple comparisons were used for the statistical evaluation of differences among means. The level of statistical significance was set at $P < 0.05$.

Chemicals and Drugs

Tel (Micardis®; $C_{33}H_{30}N_4O_2$; 4'-[(1,4'-dimethyl-2'-propyl[2,6'-bi-1H-benzimidazol]-1'-yl)-1'-yl] methyl)-[1,1'-biphenyl]-2-carboxylic acid), bisphenol A diglycidyl ether (BADGE) and ciglitazone were obtained from Tocris Cookson Ltd. (Bristol, UK), and angiotensin II, tefluthrin, tetraethylammonium chloride (TEA), tetrodotoxin and valsartan were from Sigma-Aldrich (St. Louis, MO). Tissue culture media and trypsin/EDTA were obtained from Invitrogen (Carlsbad, CA). All other chemicals including $CdCl_2$, CsCl and CsOH were commercially available, and they were prepared from reagent-grade chemical and Milli-Q water.

Computer Simulations

To simulate the slowing in the rate of I_{Na} inactivation, a modified Hodgkin-Huxley (HH) model was mathematically constructed. The theoretical model used in this study was described previously (4, 6, 45). For total I_{Na}, the modified HH scheme (*i.e.*, m^3h formalism) was used according to the following equation:

$$I_{Na} = G_{Na} \times m^3 \times h \times (V - V_{Na})$$

The rate constants for I_{Na} implemented in the simulation here are described by the following equations:

$$\alpha_m = \frac{0.1(V+40)}{1-\exp[-0.09(V+40)]},$$
$$\beta_m = 4\exp[-0.055(V+65)],$$
$$\alpha_h = 0.07ex[-0.05(V+65)],$$
$$\beta_h = \frac{1}{1+\exp[-0.1(V+35)]}.$$

The inactivation parameter of I_{Na} used for mimicking the effect of Tel on this current is reformulated by

$$h = \frac{\phi \times \alpha_h}{\alpha_h + \beta_h}$$

where h is inactivation gating variable, α_h and β_h are the rate constants for inactivation gating variable, and the parameter ϕ represents the magnitude of Na_V-channel inactivation. As the value of ϕ is elevated, the time course of Na_V channel inactivation elicited by membrane depolarization becomes

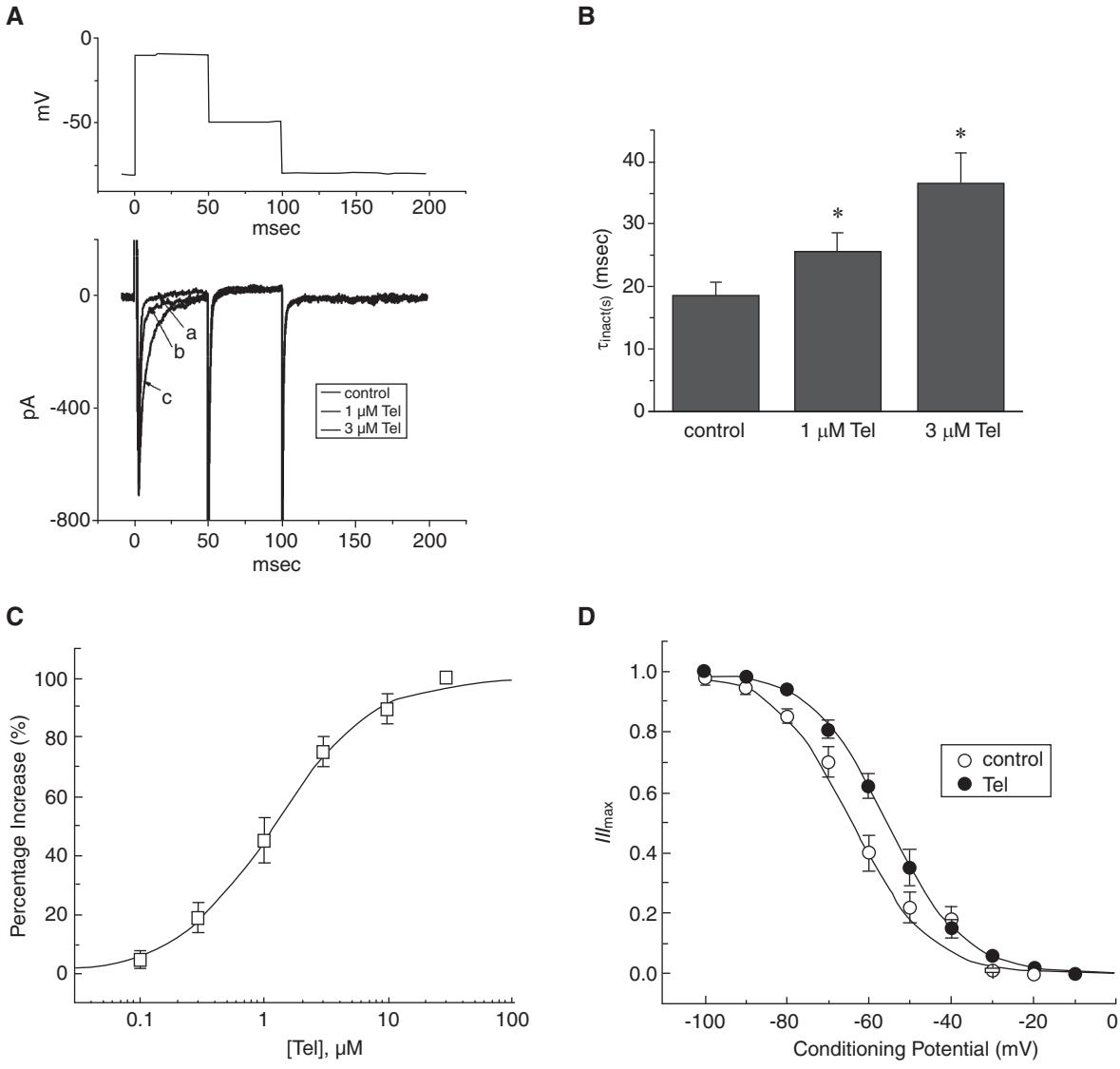

Fig. 1. Stimulatory effect of Tel on voltage-gated I_{Na} in differentiated NSC-34 neuronal cells. In this set of experiments, NSC-34 cells were immersed in Ca^{2+}-free Tyrode's solution which contained 0.5 mM $CdCl_2$ and 10 mM TEA, and the recording pipettes were filled with Cs^{+}-containing solution. (A) Superimposed I_{Na} traces obtained in the absence (a) and presence of 1 μM (b) or 3 μM (c) Tel in an NSC-34 cell. The upper part in (A) indicates the voltage protocol applied to the examined cell at a rate of 0.1 Hz. (B) Summary of the data showing effects of Tel on the time constant for the slow component of I_{Na} inactivation ($\tau_{inact(S)}$) elicited by membrane depolarization from -80 to -10 mV. Each bar represents means ± SEM of data from 12 cells. *Significantly different from control ($P < 0.05$). Note that the presence of Tel can prolong the value of $\tau_{inact(S)}$ as well as enhance the peak I_{Na} amplitude. (C) Concentration-response relationship of Tel-induced stimulation of peak I_{Na} (means ± SEM; n = 8-12 for each point). The smooth line represents the best fit to the Hill equation as described in Materials and Methods. The values for EC_{50}, Hill coefficient, and maximal percentage increase of I_{Na} were 1.2 μM, 1.1, and 100%, respectively.

slowed along with increased current amplitude.

Changes of membrane potential in this modified HH model are described by the following equation:

$$C_m \frac{dV}{dt} = -I_{Na} - I_K - I_L$$

where C_m is the membrane capacitance and V is the membrane potential. The model equation used to formulate other types of ionic currents (*e.g.*, I_K and I_L) were previously described (6, 35).

Computer programs shown in this study were either written in C++ programming language or came with the XPP simulation package available at http://www.math.pitt.edu/~bard/xpp/xpp.html, at which the analyses for linear stability and bifurcation were

Table 1. Default parameter values used for the modified HH model in this study.

Symbol	Description	Value
C_m	Membrane capacitance	1 μF
G_{Na}	Maximal I_{Na} conductance	120 mS/cm^2
G_K	Maximal K^+ current conductance	36 mS/cm^2
G_L	Leak current conductance	0.3 mS/cm^2
V_{Na}	Na^+ reversal potential	+50 mV
V_K	K^+ reversal potential	-77 mV
V_L	Reversal potential for leak current	-54.4 mV

primarily performed. Parts of numerical simulations such as I_{Na} were verified under Microsoft Excel (4, 34). They were run under a Hewlett-Packard workstation (HPxw9300; Palo Alto, CA). The ordinary differential equations were numerically solved using the explicit Euler method with a time step of 0.01 msec. In the present simulations, the values of ionic conductance and reversal potential used to solve the set of ordinary differential equations are listed in Table 1, unless otherwise stated. Source files applied for this study can be available at http://senselab.med.yale.edu/modeldb. For the sake of clarity, figures shown in this paper were made in OriginPro 2016 (Microcal Software, Inc., Northampton, MA).

Results

Effect of Tel on I_{Na} in NSC-34 Neuronal Cells

The first set of experiments was conducted to investigate the possible effect of Tel on I_{Na} in response to step depolarizations in these cells. Cells were immersed in Ca^{2+}-free Tyrode's solution to which 0.5 mM $CdCl_2$ and 10 mM TEA were added, and the whole-cell voltage-clamp experiments were made with Cs^+-containing pipette solution. $CdCl_2$ and TEA are known to block Ca^{2+} and K^+ currents, respectively. As shown in Fig. 1, the cell was depolarized from -80 to -10 mV with a duration of 50 msec, and the rapidly activating I_{Na} which was sensitive to block by tetrodotoxin (1 μM) could be readily elicited. Interestingly, when cells were challenged with Tel, the peak amplitude of I_{Na} was significantly enhanced and the inactivation time course of this current became greatly slowed. For example, when the step depolarization was applied from -80 to -10 mV, addition of Tel at a concentration of 3 μM significantly increased the peak amplitude of I_{Na} from 413 ± 15 to 698 ± 23 pA (n = 12, $P < 0.05$). Besides that, the slow component for the inactivation time constant of I_{Na} ($\tau_{inact(S)}$) was significantly prolonged to 36.5 ± 2.3 msec (n = 12, $P < 0.05$) from a control of 18.6 ± 1.5 msec (Fig. 1B). After washout of the drug, I_{Na} amplitude was returned to 432 ± 19 pA (n = 9). Similarly, addition of tefluthrin (10 μM), a pyrethroid with the I_{Na}-stimulating activities (36, 37), could increase the peak I_{Na} accompanied by a considerable reduction in I_{Na} inactivation observed in these cells.

The relationship between the concentration of Tel and the percentage increase of peak I_{Na} was constructed (Fig. 1C). The presence of Tel (0.1-30 μM) was found to increase the peak amplitude of I_{Na} in a concentration-dependent manner. The half-maximal concentration required for the stimulatory effect of Tel on I_{Na} was 1.2 μM; and Tel at a concentration of 30 μM increased peak I_{Na} fully. The Hill coefficient was noted to be 1.1, suggesting that there was no cooperativity involved.

To characterize stimulatory effect of Tel on I_{Na} in NSC-34 neuronal cells, we also explored whether there are any changes in the inactivation curve of I_{Na} during cell exposure to this compound. Fig. 1D showed the steady-state inactivation curves of I_{Na} obtained following the application of Tel (3 μM). The relationship between the conditioning potentials and the normalized amplitudes of I_{Na} was derived and fitted with a Boltzmann function. Values of voltage for half-maximal inactivation ($V_{1/2}$) and corresponding slope factor (k) in the control were -64.2 ± 1.1 and 9.3 ± 0.2 mV (n = 9), respectively, while during the exposure to 3 μM Tel, those of $V_{1/2}$ and k were -55.6 ± 1.2 and 9.2 ± 0.2 mV (n = 9), respectively. As a result, the results demonstrated that the steady-state inactivation curve of I_{Na} during the exposure to Tel was significantly shifted to a rightward direction, with no clear change in the slope factor (k value) of this curve.

Simulated I_{Na} Traces Created from a Modified HH Model

In order to closely mimic the stimulatory action of Tel on I_{Na} observed in NSC-34 cells, we further investigated how the amplitude and gating of I_{Na} can be modified to influence the electrical behavior of neurons. The modeled I_{Na} was then created on the basis of a modified HH model (6, 34). In this set of simulations, the values of G_{Na} and V_{Na} were set to be 120 mS/cm^2 and +50 mV, respectively, while the initial values of m and h are 0.052 and 0.596, respectively. Under these conditions, when the h inactivation gating value (*i.e.*, the ϕ value) was increased in a stepwise fashion, the peak amplitude of modeled I_{Na} elicited in response to step depolarization from -80 to -10 mV was clearly increased along with a progressive slowing

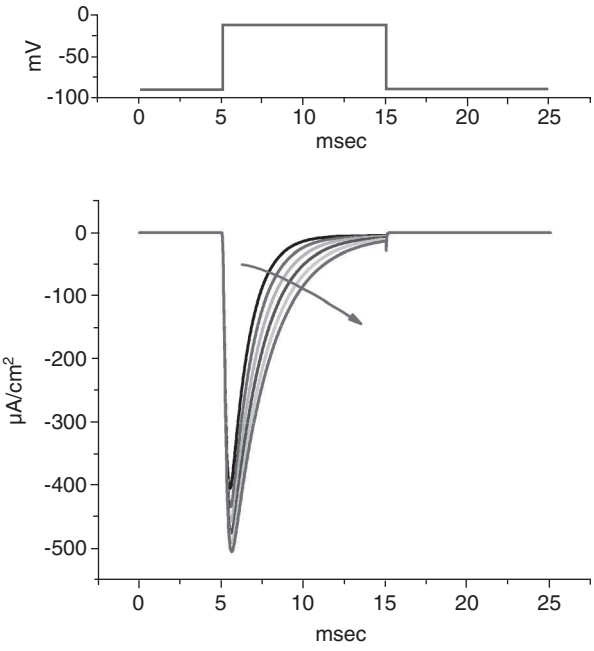

Fig. 2. Simulated I_{Na} traces in response to membrane depolarization. Detailed simulation profile on the basis of a modified HH model was described in Materials and methods. I_{Na} traces were created when the ϕ value in the inactivation gating variable (h) was increased from 1.0 to 2.0 with 0.2 increments (as indicated by curved arrow). The upper part indicates the voltage protocol used.

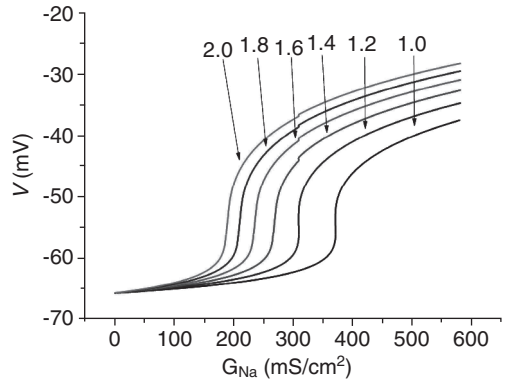

Fig. 3. Steady-state of V plotted against the value of G_{Na}. Each arrow indicates the value of ϕ (from 1.0 to 2.0 with 0.2 increments) for the inactivation gating variable (h). Of note, although the overall relationship of G_{Na} versus V remains unchanged, the curve was shifted towards leftward and upward as the ϕ value was increased in a stepwise fashion.

in I_{Na} inactivation (Fig. 2). It is established that a stepwise 0.2 increase of the ϕ value embedded in h inactivation variable is capable of decreasing the inactivation rate of I_{Na} accompanied by a gradual increase of peak I_{Na}. It is therefore clear that current trajectories tend to correspond well with the experimental results showing that Tel induced stimulation of I_{Na} seen in NSC cells (Fig. 1).

Relationship of Changes in Steady-State V Versus the G_{Na} Value

The change of steady-state V as a function of G_{Na} was further investigated in this biophysical model. In this set of simulation, G_{Na} was taken as a variable, and the other parameters were kept with default values shown in Table 1. For example, at ϕ = 1, as the G_{Na} value increased, the V became gradually depolarized (Fig. 3). When the G_{Na} value was below 300 mS/cm^2, V was changed slowly; however, as G_{Na} was larger than 350 mS/cm^2, V became rapidly depolarized. In other words, under this condition, the equilibrium point was sensitive to G_{Na} value, when this value ranged from 350 to 550 mS/cm^2. Results from this simulation point out that a slight change of G_{Na} in this range may lead the model to a totally different state. For example, at G_{Na} = 100 mS/cm^2, the eigenvalues (*i.e.*, λ) of the linearized system (8) were -4.624843, -0.119834, -0.238660 + 0.373605i, and -0.238660 – 0.373605i, the last two of which are the complex conjugate pair with negative real parts; however, at G_{Na} = 400 mS/cm^2, those values were -12.657916, -0.259931, 3.579923, and 0.044399.

As the bifurcation theory was further applied (9, 45), one bifurcation point (*i.e.*, G_{Na} = 212.6 mS/cm^2) was established when G_{Na} varied. The results obtained reflected that the model underwent a Hopf bifurcation as G_{Na} reached this value and that a periodic solution could emanate from this point. The system is stable around equilibrium when G_{Na} is less than this value, while it becomes unstable as the bifurcation point for G_{Na} is exceeded. When the stability of the model was analyzed at G_{Na} = 212.6 mS/cm^2 and other parameters were set at desired values, the eigenvalues were computed to be -4.971929, -0.125961, 0.000359 + 0.380179i, and 0.000359 – 0.380179i, the last two values of which can be approximately regarded as 0.

Afterwards, we increased the ϕ value stepwise by 0.2; and, the relationship of steady-state V versus G_{Na} was notably shifted toward the left. For example, at ϕ = 2, when G_{Na} reached 180 mS/cm^2, an abrupt depolarization clearly occurred, although potential change was notably slowed when G_{Na} was less than 180 mS/cm^2. The equilibrium point became sensitive to G_{Na} as this value was greater than 180 mS/cm^2. Based on the bifurcation theory, at ϕ = 2, the point of Hopf bifurcation became shifted to 106.2 mS/cm^2. At ϕ = 2 and G_{Na} = 106.2 mS/cm^2, the eigenvalues obtained under this condition were -4.971545, -0.067198, 0.000342 + 0.368152i, and 0.000342 –

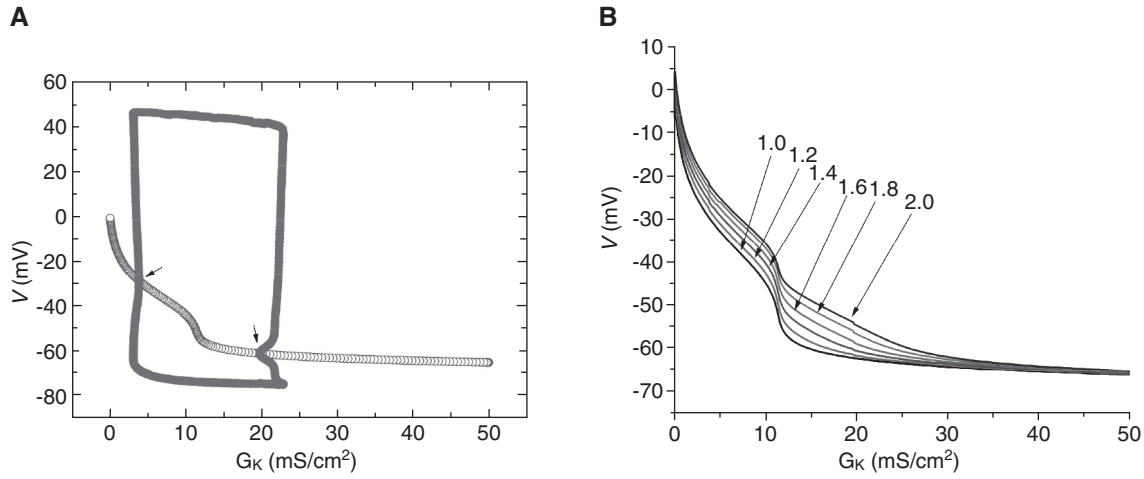

Fig. 4. Bifurcation diagram of G_K versus V (A) and steady-state of V plotted against the G_K value (B). In this diagram (A), the ϕ value for h inactivation gating variable was set at 1.0. The open circles represents the equilibrium state, whereas red color is a periodic solution indicating that there is spontaneous firing in the model. Arrows indicate the hopf bifurcation point (*i.e.*, subcritical [3.84 mS/cm^2] and supercritical [19.76 mS/cm^2] bifurcation points). In (B), each arrow indicates the value of ϕ (from 1.0 to 2.0 with 0.2 increments) included in the inactivation gating variable (h). Of note, although the overall relationship of G_K versus V remains unchanged, the curve was progressively shifted to the rightward and upward direction after each stepwise increase of the ϕ value. The corresponding values of bifurcation points were shifted to a rightward direction as the ϕ value was increased.

0.368152i, the complex numbers of which are taken to be 0. Therefore, stepwise increase of the ϕ value can alter effect of G_{Na} on the stability analyzed in this model.

Relationship of Changes in Steady-State of V Versus the G_K Value

Next, we chose G_K as a variable and kept the other parameters with default values shown in Table 1. The same method for the analysis of G_{Na} was taken to explore the effect of G_K on the equilibrium, stability and bifurcation of this HH model. Because the desired value of G_K was 36.0 mS/cm^2 (Table 1), the value of G_K was appropriately chosen to range between 0 and 50 mS/cm^2. As ϕ = 1, the relationship between G_K and the change of V is illustrated in Fig. 4. Notably, unlike the value for G_{Na} which displayed only one critical one, there were two critical values about G_K (*i.e.*, the subcritical and supercritical bifurcation points). The G_K values of subcritical and supercritical points obtained at ϕ = 1 were computed to be 3.84 and 19.76 mS/cm^2, respectively. At G_K = 3.84 mS/cm^2, the eigenvalues of the model were computed to be -5.321428, -0.422595, -0.000024 + 1.130357i, and -0.000024 – 1.130357i, while at G_K = 19.76 mS/cm^2, those were -4.537836, -0.131896, 0.000475 + 0.343883i, and 0.000475 – 0.343883i. As the G_{Na} values ranged between subcritical and supercritical points, there appeared to a stable limit cycle (*i.e.*, an isolated closed trajectory in the phase plane) inherently in this modified HH model, despite no current injection given (Fig. 4A). These results can be interpreted to mean that the model is stable when G_K is less than the subcritical point and greater than the supercritical point. However, there are self-sustained and periodic oscillations at a certain frequency when the G_K value falls to the range between subcritical and supercritical points.

However, when the ϕ value in h inactivation gating value was progressively increased, these two values placed at the bifurcation points were elevated (Fig. 4B). For example, as ϕ = 2.0, the subcritical and supercritical points for G_K became 5.65 and 40.77 mS/cm^2, respectively. At G_K = 5.65 mS/cm^2 and ϕ = 2.0, the eigenvalues obtained were -7.039552, -0.379649, 0.000445 + 1.168882i, and 0.000445 – 1.168882i, while at G_K = 40.77 mS/cm^2 and ϕ = 2, those were -5.068220, -0.066499, 0.0004888 + 0.376045i, and 0.0004888 – 0.376045i. Therefore, stepwise increase of the ϕ value inside the h inactivating variable apparently increased the values of bifurcation points and the range between two bifurcation points became progressively widened.

Changes of V and Relationship of m, h and n

Changes in V given at different ϕ values were further determined. As shown in Fig. 5A, the ϕ value was set at 1.0, the value of G_{Na} was arbitrarily set at 190 mS/cm^2 and V was plotted over time. It is noted that the trajectory of V slightly fluctuated and was

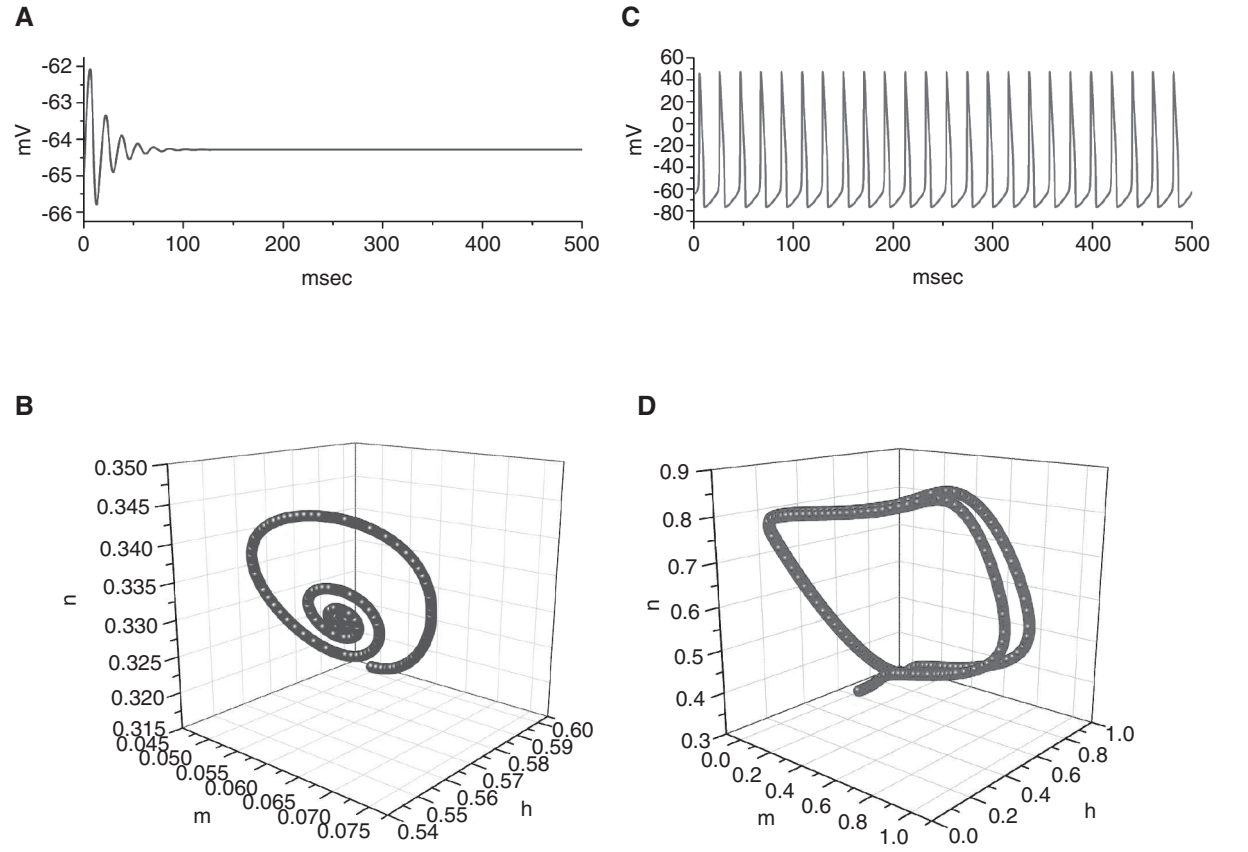

Fig. 5. Changes in V as a function of time (panels A and C) and three-dimensional trajectories for the relationship of m, n, and h (panels B and D). In this set of simulation, the value of G_{Na} was set at 190 mS/cm^2, and other parameters were given at the default values (Table 1). The ϕ values for h inactivation gating variable are set to be 1.0 (panels A and B) and 2.0 (panels C and D), respectively.

followed by an equilibrium state eventually. The corresponding change in the trajectory of gating variables m, h, and n with time is illustrated in Fig. 5B. It is clear that the electrical behavior of the modeled cell can spiral eventually toward an equilibrium state. The reason from this result is due to the fact that the G_{Na} value of 190 mS/cm^2 is less than the value for bifurcation point (212.6 mS/cm^2). When G_{Na} = 190 mS/cm^2, ϕ = 1.0 and other parameters were set at default values, the eigenvalues were -4.997662, -0.124380, -0.055984 + 0.390982i, and -0.055984 – 0.390982i, the last two of which were noted to be complex numbers with negative real parts (*i.e.*, stable focus). Correspondingly, the maximal Lyapunov exponent, a measure of chaos, was calculated to be was -0.0556363.

However, as the ϕ value was set to 2.0, the system became unstable and the periodical change in V occurred (Fig. 5C and 5D). Notably, as the ϕ value was at 2.0, the system was perturbed and the bifurcation point of G_{Na} value was shifted to 106.2 mS/cm^2, a value that became lower than 190 mS/cm^2. Consequently, the repetitive firing of APs appeared (Fig. 5C) and the trajectory of m, h, and n with time turned out to be circles eventually (Fig. 5D). Under this condition, the system became unstable and the electrical activity of cells was in a periodical state at a certain frequency. When G_{Na} = 190 mS/cm^2, ϕ = 2, and other parameters were set at default values, the eigenvalues were -11.301138, -0.181231, 3.742668, and 0.011457, and the maximal Lyapunov exponent became positive (*i.e.*, 0.241989). Therefore, when there is the stepwise increase of ϕ value, in which stimulatory effect of Tel on I_{Na} is mimicked, the firing tendency of modeled cell is virtually increased.

Similarly, when the ϕ value in h inactivation variable was 1.0, G_K was arbitrarily set to 25 mS/cm^2 and other parameters were set at desired values, the system remains to be stable because, under this condition, the G_K value became greater than the supercritical bifurcation point (19.76 mS/cm^2). Indeed, as G_K = 25 mS/cm^2 with the default values in other parameters, the calculated eigenvalues were -4.567741, -0.125725, -0.095417 + 0.372708i, and -0.095417 – 0.372708i, the last two of which notably had negative real parts. However, as ϕ was increased

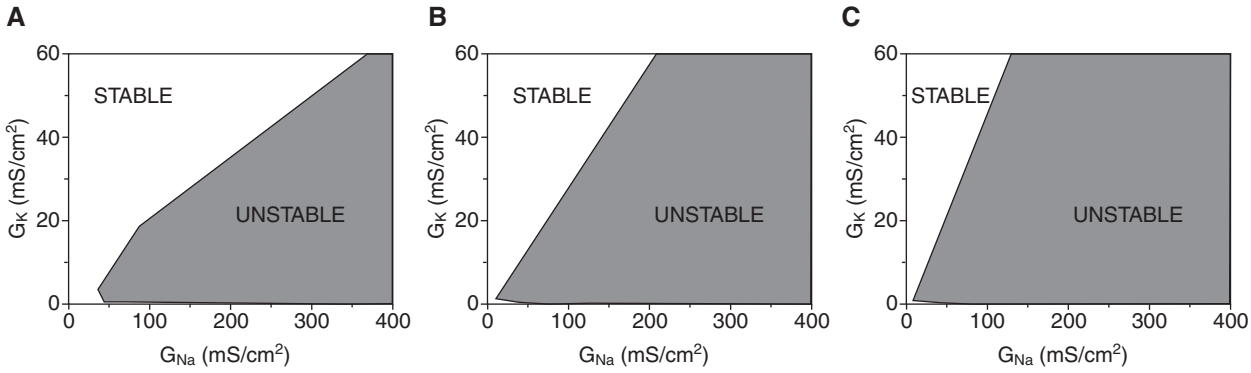

Fig. 6. Excitability diagram of G_{Na} and G_K existing in modified HH model. The shaded gray region indicates the unstable state which is able to produce periodical solutions in a certain period, while the white region represents the stable state. The black solid line indicates the critical boundary. The value of ϕ for inactivation gating variable (h) in (A) is 1.0 and those shown in (B) and (C) are 2.0. In (C), the ϕ value of h gating variable is set at 2.0 and the V_K value is -50 mV to mimic the elevation of extracellular K^+ concentration.

to 2.0, repetitive firing of APs occurred because the G_K value fell to the range between two bifurcation points (*i.e.*, 5.65 and 40.77 mS/cm^2). As G_K = 25 mS/cm^2 and ϕ = 2, the eigenvalues were -5.641992, -0.105577, 1.127239, and 0.027936.

Phase Plane of G_{Na} and G_K Derived from this HH Model

The effects of G_{Na} and G_K on the stability and bifurcation of modeled HH cells were further analyzed. As shown in Fig. 6, according to the stability theory (9), it is anticipated that the model becomes stable when G_{Na} and G_K are in white region and it turns out to be unstable when G_{Na} and G_K fall to gray region. The means that the electrophysiological activity can reach a steady state as G_{Na} and G_K are in white region; however, change in V becomes periodic, when the values of these two conductances are placed at gray region. The stability of the model was further analyzed. When eigenmatrix and eigenvalues of the model were computed, we further found out that the real parts in the complex numbers for all of its eigenvalues were negative if G_{Na} and G_K were placed at white region shown in Fig. 6. However, if G_{Na} and G_K belonged to gray region, positive real numbers in eigenvalues clearly appeared. For example, as G_{Na} = 190 mS/cm^2 and G_K = 10 mS/cm^2 which are placed at gray region, the eigenvalues are -0.120304, -0.372698, 0.593699 + 0.709043i, and 0.593699 – 0.709043i, the last two of which are positive real parts. However, as G_{Na} = 190 mS/cm^2 and G_K = 40 mS/cm^2 which are in white region, the corresponding eigenvalues are -4.90174, -0.122658, -0.100206 + 0.400234i, and -0.100206 – 0.400234i and the periodical changes resultantly vanish.

As depicted in Fig. 6, the results led us to indicate that when G_{Na} and G_K are in white region, the electrophysiological activity can reach a steady state; however, as G_{Na} and G_K belong to gray region, the activity becomes periodic at a certain frequency. It is thus clear that the system undergoes bifurcations when G_{Na} and G_K are on the boundary (indicated by black solid line). However, when the ϕ value in h inactivation gating value was set at 2.0 and other parameters were kept in desired values, the critical boundary was shifted leftward and upward, indicating that the model becomes more unstable and is qualitatively susceptible to shift towards periodic changes in electrical behavior of cells. For example, as ϕ = 2.0, G_{Na} = 190 mS/cm^2 and G_K = 40 mS/cm^2 which become placed at gray region, the eigenvalues are -0.6.074081, -0.093835, 1.141662, and 0.038552. By virtue of a linear regression, the critical boundary of G_{Na} versus G_K at ϕ = 1.0 and ϕ = 2.0 can be expressed as $G_K = 0.161244 \times G_{Na} + 0.5743$ and $G_K = 0.29212 \times G_{Na} – 2.115329$, respectively. As a result, it is clear that the slope value increased from 0.161244 to 0.29212 when the ϕ value was elevated from 1.0 to 2.0. This value at ϕ = 2.0 is nearly twice as much as that at ϕ = 1.0.

Additionally, as hyperkalemia may occur during Tel administration (41) and elevated extracellular K^+ can alter the V_K value in HH model (26, 33, 36), we further investigated if there are any changes in the phase plane of G_{Na} and G_K. As illustrated in Fig. 6C, as ϕ = 2 and V_K = -50 mV, the critical boundary was shifted leftward further along with a broadening of unstable region created from phase plane of G_{Na} and G_K. The results indicate that this condition, where ϕ is increased, renders modeled neuron vulnerable to the appearance of repetitive firing. For example, as ϕ = 2.0, V_K = -50 mV, G_{Na} = 90 mS/cm^2 and G_K = 30 mS/cm^2 which become notably placed at gray region, the eigenvalues are

-11.958960, -0.282983, 0.094042 + 0.735902*i*, and 0.094042 – 0.735902*i*.

Simulation of Tel-Mediated Activation of I_{Na} Derived from a Markovian Model

To further elucidate the ionic mechanism of stimulatory actions of Tel, a modified markovian model used to simulate I_{Na} was examined. This model illustrated in Fig. 7A was originally derived from Clancy and Rudy (7). The detailed meanings for default parameters used in this model were described in the paper of Clancy and Rudy (7). Basically, the model consists of three closed states, one open state, one fast inactivation (IF) state, two closed-inactivation state and two intermediate inactivated states. As shown in Fig. 7B, the stimulatory effect of Tel on simulated I_{Na} was found to closely resemble the experimental observations. The results showed that the stimulatory effect of Tel at a concentration of 10 and 30 μM can be mimicked by a reduction of α_2 (*i.e.*, transitional rate from IF to open (O) state) to 19 and 10 msec^{-1} from a control vale of 29.6 msec^{-1}. Therefore, a progression toward the activated state became slowed in the presence of 10 and 30 μM Tel by 36 and 66%, respectively. The simulation results are well fit to the experimental observations showing that during cell exposure to Tel (10 and 30 μM), current amplitudes of I_{Na} in response to step depolarization were increased, along with an increase in inactivation time constant.

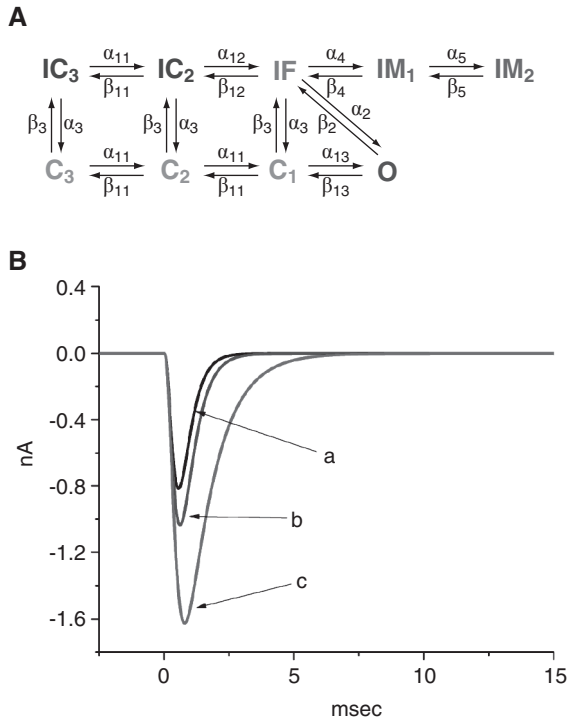

Fig. 7. Simulation of Tel-mediated activation of voltage-gated I_{Na}. The state diagram of markovian model for I_{Na} illustrated in (A) were originally developed by Clancy and Rudy (7). Source file for the formulation is available at http://senselab.med.yale.edu/senselab/modeldb. The solutions to the ordinary differential equations were implemented in XPP software package. The default values (*i.e.*, in the control) for numerical parameters are shown in the paper of Clancy and Rudy (7). In (A), C: Closed state; O: Open state; IF: Fast inactivation state; IC: Closed-inactivation state; IM: Intermediate inactivation state. In (B), the model cell was depolarized from -80 to -10 mV. When the value of α_2 was changed to 19 msec^{-1} (b) and 10 msec^{-1} (c) from a control value of 20.6 msec^{-1} (a), there was an increase in peak amplitude in combination with the increased inactivation time constant. Traces (b) and (c) were created to mimic the effect of 10 and 30 μM Tel, respectively. IF $\leftrightarrow$ O is linked to the fast inactivation, while IF $\leftrightarrow$ IM_1 and IM_1 $\leftrightarrow$ IM_2 correspond to the slow inactivation process.

Discussion

The principal findings of this study were that, in differentiated NSC-34 neuronal cells, addition of Tel consistently increased the peak amplitude of I_{Na} and the inactivation time constant of this current; however, it did not alter the activation time course of the current. The simulation model presented herein was used to predict that a delay in the inactivation time course of I_{Na} (*i.e.*, *h* inactivating variable) can mainly modify the stability and bifurcations of G_{Na} and G_K. Taken together, findings from this study reveal that the increases of both peak amplitude and inactivation time constant of I_{Na}, in which the Tel action is mimicked, are the potential mechanisms underlying the rate and pattern of repetitive firing of neuronal APs occurring *in vivo*.

Earlier studies have demonstrated the ability of Tel to induce agnostic activity of PPAR-γ (3, 24, 31, 40, 41, 44). Ciglitazone (3 μM), a thiazolidinedione ligand known to be an agonist of PPAR-γ (16, 36), alone had minimal effect on the amplitude and kinetics of I_{Na} in NSC-34 cells. In continued presence of Tel, subsequent application of neither angiotensin II (200 nM) nor BADGE (3 μM), an antagonist of PPAR-γ, was found to have any effect on reversing Tel-mediated stimulation of I_{Na} in this study. Additionally, in NSC-34 cells incubated with angiotensin II for 6 h, Tel-induced activation of peak I_{Na} and slowing in current inactivation remained intact (data not shown). Valsartan (3 μM), another blocker of AT1R, also stimulated I_{Na} effectively in NSC-34 cells. Therefore, it is likely that the actions of Tel or other structurally similar compounds on I_{Na} seen in NSC-34 cells are largely in-

dependent of either its binding to AT1Rs or activation of PPAR-γ. Although the exact binding target for Tel is currently unclear, the challenge of cells (*e.g.*, NSC-34 neuronal cells) with Tel can exert an interaction at binding site(s) inherently existing on Na_V channels, resulting in conformational changes in the channel protein and eventually perturbing the gating kinetics of the channel. In other words, activation of I_{Na} by Tel is not instantaneous, but develops with time after the channel becomes opened, thereby producing a slowing in current inactivation. Moreover, there is a rightward shift of steady-state inactivation curve of I_{Na} during cell exposure to Tel.

The changes in the qualitative nature of solutions to HH-based differential equations as the parameters of ϕ, G_{Na} and G_K varies are demonstrated in this study. In numerical simulation, as compared with those at ϕ = 1, the peak amplitude of I_{Na} is actually enhanced in combination with a marked slowing in I_{Na} inactivation when ϕ is arbitrarily chosen at 2.0. These theoretical results clearly indicate that changes in the magnitude and kinetics of Na_V channels, in which ϕ value varies and the Tel action is mimicked, can cause significant impact on electrical behavior of neurons or neuroendocrine cells occurring *in vivo*. Additionally, by virtue of a markovian model for I_{Na} (7), the simulated I_{Na} was also created to mimic the stimulatory action of Tel on this current.

Our study showed that, when the retardation of I_{Na} inactivation on which addition of Tel produced an action occurred, the relationship of steady-state change in V versus G_{Na} became progressively altered. Stable states shown in this study predict that the electrophysiological activity of cell (*e.g.*, NSC-34 neuronal cell) will get to corresponding resting state eventually, while periodic phenomenon tends to be similar to the response of pathological cell's APs caused by cardiac arrhythmias (27, 28). Besides that, under this condition, the relationship of changes in V versus G_K still remained to be markedly altered, despite no changes in the default parameter values inherently from modeled I_K. Nonetheless, Tel is able to exert an additional unanticipated effect on the amplitude and kinetics of I_{Na} in neurons, which is presumably independent of blockade of AT1Rs. Similarly, (-)-epicatechin-3-gallate or tefluthrin were recently reported to be an agonistic action on I_{Na} accompanied by the decreased inactivation rate (14, 32, 38, 39). The data also implied the possibility of Tel actions on other types of excitable cells that express functional Na_V channels (18).

The biophysical model used in this study tends to be based on a relatively small number of variables. However, it indeed allows us to highlight a qualitative way how neurons or neuroendocrine spike and why they switch between two modes of firing without any need of knowing the detailed scheme in the system (27). The quantitative model presented herein is able to complement the experimental observations by providing insight into Na_V channels, which can impinge upon electrical behavior of neurons or neuroendocrine cells. Our stimulation results generated from this model also support the notion that changes in the magnitude and kinetics of I_{Na} caused by Tel, in which varying ϕ is one of the valuable parameters, are responsible for its actions on the functional activity of neurons or neuroendocrine cells *in vivo*. Taken together, it should be noted here that the neurological actions caused by Tel or its structurally similar compounds can be linked mainly to its direct actions on the amplitude and gating of Na_V channels (18). Attention therefore needs to be given in attributing Tel-induced neurological actions *in vivo* to either blockade of AT1R or activation of PPAR-γ activity (1-3, 13, 19, 20, 29, 30, 44). The majority of I_{Na} identified in differentiated NSC-34 neuronal cells was found to resemble $Na_V1.7$ encoded by SCN9A gene. Whether Tel-induced stimulation of I_{Na} is isoform-specific remains to be further explored.

In this study, two theoretical models were used for investigations on Tel actions on the kinetics of I_{Na} recorded from NSC-34 neuronal cells. Indeed, on the basis of our simulations, these two models were found to mimic the effect of Tel on I_{Na}, although there are three inactivated states in the model of Clancy and Rudy (7). It is therefore possible that the Tel molecule acts predominantly on the fast inactivated state of Na_V channels. However, the Clancy Rudy model (7) is tailored to the cardiac $Na_V1.5$ channel, not to neuronal Na_V channels. Therefore, whether the Tel molecule contributes to the slow inactivated states in Na_V channels remains to be further experimentally explored.

In this study, addition of Tel enhanced I_{Na} with an EC_{50} value of 1.2 μM. The plasma Tel concentration after oral and intravenous administration of a single dose of 40 mg Tel can reach about 0.087 μM (44.7 ng/ml) and 2.32 μM (1196 ng/ml), respectively (26). The plasma level of Tel reported previously (26) was obtained after intravenous administration which is not usually done in clinical setting. Therefore, under such conditions, or, perhaps, with oral overdosing, Tel would have a substantial effect on I_{Na}. Moreover, binding studies performed in membrane preparations derived from rat lung have reported a high affinity of Tel to the AT1R with a Ki value of 3.7 nM (12). Tel concentrations in the cerebrospinal fluid (CSF) following 8 days of oral treatment with lowest and highest (1 and 30 mg/kg of body weight per day) were reported to range from 0.9 ng/ml to 46.5 ng/ml (*i.e.*, from 2 to 100 nM) (12). Because the Tel molecule pos-

sesses good lipophilicity, it can readily transverse the blood-brain barrier and subsequently penetrate different brain regions. Therefore, to what extent Tel-stimulated I_{Na} presented herein could be of pharmacological relevance remains to be further delineated.

Acknowledgments

This study was supported by a grant from National Cheng Kung University under Grant no. 1030101. Many thanks are due to Yan-Ming Huang and Yu-Kai Liao for their technical assistances in the earlier experiments.

Conflict of Interest

The authors declare that they have no competing interests.

References

1. Balaji, S.P., Chand, C.V., Justin, A. and Ramanathan, M. Telmisartan mediates anti-inflammatory and not cognitive function through PPAR-γ agonism *via* SARM and MyD88 signaling. *Pharmacol. Biochem. Behiav*. 137: 60-68, 2015.
2. Benigni, A., Cassis, P. and Remuzzil, G. Angiotensin II revisited new roles in inflammation, immunology and aging. *EMBO Mol. Med*. 2: 247-257, 2010.
3. Benson, S.C., Pershadsingh, H.A., Ho, C.I., Chittiboyina, A., Desai, P., Pravenec, M., Qi, N., Wang, J., Avery, M.A. and Kurtz, T.W. Identification of telmisartan as a unique angiotensin II receptor antagonist with selective PPARγ-modulating activity. *Hypertension* 43: 993-1002, 2004.
4. Brown, A.M. A modeling study predicts the presence of voltage gated Ca^{2+} channels on myelinated central axons. *Comput. Meth. Prog. Biomed*. 71: 25-31, 2003.
5. Catterall, W.A., Goldin, A.L. and Waxman, S.G. International union of pharmacology. XXXIX, Compendium of voltage-gated ion channels: sodium channels. *Pharmacol. Rev*. 54: 575-578, 2003.
6. Chen, B.S., Lo, Y.C., Liu, Y.C. and Wu, S.N. Effects of transient receptor potential-like current on the firing pattern of action potentials in the Hodgkin-Huxley neuron during exposure to sinusoidal external voltage. *Chinese J. Physiol*. 53: 423-429, 2010.
7. Clancy, C.E. and Rudy, Y. Na^+ channel mutation that causes both Brugada and long-QT syndrome phenotypes: a simulation study of mechanism. *Circulation* 105: 1208-1213, 2002.
8. Du, G.T., Hu, M., Mei, Z.L., Wang, C., Liu, G.J., Hu, M., Long, Y., Miao, M.X., Li, J.C. and Hong, H. Telmisartan treatment ameliorates memory deficits in streptozotocin-induced diabetic mice *via* attenuating cerebral amylodosis. *J. Pharmacol. Sci*. 124: 418-426, 2014.
9. Fall, C.P., Marland, E.S., Wagner, J.M. and Tyson, J.J. *Computational Cell Biology*. Springer, New York, 2002.
10. Farsang, C. Indications for and utilization of angiotensin receptor II blockers in patients at high cardiovascular risk. *Vasc. Health Risk Manag*. 7: 605-622, 2011.
11. George, J., Baden, D.G., Gerwick, W.H. and Murray, T.F. Bidirectional influence of sodium channel activation and NMDA receptor-dependent cerebrocortical neuron structural plasticity. *Proc. Natl. Acad. Sci. USA* 109: 19840-19845, 2012.
12. Gohlke, P., Weiss, S., Jansen, A., Wienen, W., Stangier, J., Rascher, W., Culman, J. and Unger, T. AT_1 receptor antagonist telmisartan administered peripherally inhibits central responses to angiotensin II in conscious rats. *J. Pharmacol. Exp. Ther*. 298: 62-70, 2001.
13. Haruyama, N., Fujisaki, K., Yamato, M., Eriguichi, M., Noguichi, H., Torisu, K., Tsuruya, K. and Kitazono, T. Improvement in spatial memory dysfunction by telmisartan through reduction of brain angiotensin II and oxidative stress in experimental uremic mice. *Life Sci*. 113: 55-59, 2014.
14. He, B. and Soderlund, D.M. Effects of the β1 auxiliary subunit on modulation of Rat $Na_V1.6$ sodium channels expressed in HEK293 cells by the pyrethroid insecticides tefluthrin and deltamethrin. *Toxicol. Appl. Pharmacol*. 291: 58-69, 2016.
15. Hsu, H.T., Tseng, Y.T., Lo, Y.C. and Wu, S.N. Ability of naringenin, a bioflanonoid, to activate M-type potassium current in motor neuron-like cells and to increase BK_{Ca}-channel activity in HEK293T cells transfected with α-*hSlo* subunit. *BMC Neurosci*. 15: 135, 2014.
16. Jha, R.J. Thiazolidinediones-the new insulin enhancers. *Clin. Exp. Hypertens*. 21: 157-166, 1999.
17. Jukič, M., Kikelj, D. and Anderluh, M. Isoform selective voltage-gated sodium channel modulators and the therapy of pain. *Curr. Med. Chem*. 21: 164-186, 2014.
18. Kim, H.K., Youm, J.B., Lee, S.R., Lim, S.E., Lee, S.Y., Ko, T.H., Longe, L.T., Nilius, B., Won, D.N., Noh, J.H., Ko, K.S., Rhee, B.D., Kim, N. and Han, J. The angiotensin receptor blocker and PPAR-γ agonist, telmisartan, delays inactivation of voltage-gated sodium channel in rat heart: novel mechanism of drug action. *Pflugers. Arch*. 464: 631-643, 2012.
19. Kono, S., Kurata, T., Sato, K., Omote, Y., Hishikawa, N., Yamashita, T., Deguchi, K. and Abe, K. Neurovascular protection by telmisartan *via* reducing neuroinflammation in stroke-resistant spontaneously hypertensive rat brain after ischemic stroke. *J. Stroke Cerebrovasc. Dis*. 24: 537-547, 2015.
20. Lin, C.M., Tsai, J.T., Chang, C.K., Cheng, J.T. and Lin, J.W. Development of telmisartan in the therapy of spinal cord injury: pre-clinical study in rats. *Drug Des. Devel. Ther*. 9: 4709-4717, 2015.
21. Lo, Y.C., Tseng, Y.T., Liu, C.M., Wu, B.N. and Wu, S.N. Actions of KMUP-1, a xanthine and piperazine derivative, on voltage-gated Na^+ and Ca^{2+}-activated K^+ currents in GH_3 pituitary tumour cells. *Brit. J. Pharmacol*. 172: 5110-5122, 2015.
22. Lukawski, K., Janowska, A., Jakubus, T. and Czuczwar, S.J. Interactions between angiotensin AT_1 receptor antagonists and second-generation antiepileptic drugs in the test of maximal electroshock. *Fundam. Clin. Pharmacol*. 28: 277-283, 2014.
23. Mogi, M., Li, J.M., Tsukuda, K., Iwanami, J., Min, L.J., Sakata, A., Fujita, T., Iwai, M. and Horiuchi, M. Telmisartan prevented cognitive decline partly due to PPAR-γ activation. *Biochem. Biophys. Res. Commun*. 375: 446-449, 2008.
24. Nagashima, A., Watanabe, R., Ogawa, M., Suzuki, J., Masumura, M., Hishikari, K., Shimizu, T., Takayama, K., Hirata, Y., Nagai, R. and Isobe, M. Different roles of PPAR-γ activity on physiological and pathological alteration after myocardial ischemia. *J. Cardiovasc. Pharmacol*. 60: 158-164, 2012.
25. Qureshi, S.F., Ali, A., John, P., Jadhav, A.P., Venkateshwari, A., Rao, H., Jayakrishnan, M.P., Narasimhan, C., Shenthar, J., Thangaraj, K. and Nallari, P. Mutational analysis of SCN5A gene in long QT syndrome. *Meta Gene* 6: 26-35, 2015.
26. Stangier, J., Schmid, J., Türck, D., Switek, H., Verhagen, A., Peeters, P.A.M., van Marle, S.P., Tamminga, W.J., Sollie, F.A.E. and Jonkman, J.H.G. Absorption, metabolism, and excretion of intravenously and orally administered [^{14}C]telmisartan in healthy volunteers. *J. Clin. Pharmacol*. 40: 1312-1322, 2000.
27. Sung, R.J., Wu, S.N., Wu, J.S., Chang, H.D. and Luo, C.H. Electrophysiological mechanisms of ventricular arrhythmias in relation to Andersen-Tawil syndrome under conditions of reduced IK1: a simulation study. *Am. J. Physiol. Heart Circ. Physiol*. 291: H2597-H2605, 2006.

28. Sung, R.J., Wu, Y.H., Lai, N.H., Teng, C.H., Luo, C.H., Tien, H.C., Lo, C.P. and Wu, S.N. Beta-adrenergic modulation of arrhythmogenesis and identification of targeted sites of antiarrhythmic therapy in Timothy (LQT8) syndrome: a theoretical study. *Am. J. Physiol. Heart Circ. Physiol*. 298: H33-H44, 2010.
29. Villapol, S., Balarezo, M.G., Affram, K., Saavedra, J.M. and Symes, A.J. Neurorestoration after traumatic brain injury through angiotensin II receptor blockage. *Brain* 138: 3299-3315, 2015.
30. Villapol, S., Kryndushkin, D., Balarezo, M.G., Campbell, A.M., Saavedra, J.M., Shewmaker, F.P. and Symes, A.J. Hepatic expression of serum amyloid A1 is induced by traumatic brain injury and modulated by telmisartan. *Am. J. Pathol*. 185: 2641-2652, 2015.
31. Wang, J., Pang, T., Hafko, R., Benicky, J., Sanchez-Lemus, E. and Saavedra, J.M. Telmisartan ameliorates glutamate-induced neurotoxicity: roles of AT_1 receptor blockade and PPARγ activation. *Neuropharmacology* 79: 249-261, 2014.
32. Wu, A.Z., Loh, S.H., Cheng, T.H., Lu, H.H. and Lin, C.I. Antiarrhythmic effects of (-)-epicatechin-3-gallate, a novel sodium channel agonist in cultured neonatal rat ventricular myocytes. *Biochem. Pharmacol*. 85: 69-80, 2013.
33. Wu, F., Mi, W., Burns, D.K., Fu, Y., Gray, H.F., Struyk, A.F. and Cannon, S.C. A sodium channel knockin mutant ($Na_V1.4$-R669H) mouse model of hypokalemic periodic paralysis. *J. Clin. Invest*. 123: 4082-4094, 2011.
34. Wu, S.N. Simulation of the cardiac action potential based on the Hodgkin-Huxley kinetics with the use of Microsoft Excel spreadsheets. *Chinese J. Physiol*. 47: 15-22, 2004.
35. Wu, S.N., Chen, B.S., Tsu, T.I., Peng, H., Wu, Y.H. and Lo, Y.C. Analytical studies of rapidly inactivating and noninactivating sodium currents in differentiated NG108-15 neuronal cells. *J. Theor. Biol*. 259: 828-836, 2009.
36. Wu, S.N., Ho, L.L., Li, H.F. and Chiang, H.T. Regulation of Ca^{2+}-activated K^+ currents by ciglitazone in rat pituitary GH_3 cells. *J. Investig. Med*. 48: 259-269, 2000.
37. Wu, S.N., Huang, Y.M., Kao, C.A., Chen, B.S. and Lo, Y.C. Investigations on contribution of glial inwardly-rectifying K^+ current to membrane potential and ion flux: an experimental and theoretical study. *Kaohsiung J. Med. Sci*. 31: 9-17, 2015.
38. Wu, S.N., Wu, Y.H., Chen, B.S., Lo, Y.C. and Liu, Y.C. Underlying mechanism of actions of tefluthrin, a pyrethroid insecticide, on voltage-gated ion currents and on action currents in pituitary tumor (GH_3) cells and GnRH-secreting (GT1-7) neurons. *Toxicology* 258: 70-77, 2009.
39. Wu, S.N., Yeh, C.C., Huang, H.C., So, E.C. and Lo, Y.C. Electrophysiological characterization of sodium-activated potassium channels in NG108-15 and NSC-34 motor neuron-like cells. *Acta Physiol. (Oxf)*. 206: 120-134, 2012.
40. Yamagishi, S.I., Matsui, T. and Nakamura, K. Possible molecular mechanisms by which angiotensin II type 1 receptor blockers (ARBs) prevent the development of atrial fibrillation in insulin resistant patients. *Horm. Metab. Res*. 40: 640-644, 2008.
41. Yamagishi, S. and Takeuchi, M. Telmisartan is a promising cardiometabolic sartan due to its unique PPAR-γ-inducing property. *Med. Hypotheses* 64: 476-478, 2005.
42. Yu, D., Chen, Y. and Hao, K. The pharmacokinetic-pharmacodynamic model of telmisartan and hydrochlorothiazide on blood pressure and plasma potassium after long-term administration in spontaneously hypertensive rats. *Fundam. Clin. Pharmacol*. 29: 543-552, 2015.
43. Yusuf, S., Teo, K., Anderson, C., Pogue, J., Dyal, L., Copland, I., Schumacher, H., Dagenais, G. and Sleight, P. Effects of the angiotensin-receptor blocker telmisartan on cardiovascular events in high-risk patients intolerant to angiotensin-converting enzyme inhibitors: a randomised controlled trial. Telmisartan Randomised AssessmeNt Study in ACE iNtolerant subjects with cardiovascular Disease (TRANSCEND). *Lancet* 372: 1174-1183, 2008.
44. Zeng, X.C., Li, X.S. and Wen, H. Telmisartan protects against microvascular dysfunction during myocardial ischemia/reperfusion injury by activation of peroxisome proliferator-activated receptor γ. *BMC Cardiovasc. Disord*. 13: 39, 2013.
45. Zhang, Y., Wang, K., Yuan, Y., Sui, D. and Zhang, H. Effects of maximal sodium and potassium conductance on the stability of Hodgkin-Huxley model. *Comput. Math. Methods Med*. 2014: 761907, 2014.